THE JOURNAL OF BIOLOGICAL CHEMISTRY VOL. 282, NO. 51, pp. 37036–37044, December 21, 2007

Solution Structure of Selenoprotein W and NMR Analysis of Its Interaction with 14-3-3 Proteins*[S]

Received for publication, July 2, 2007, and in revised form, September 21, 2007 Published, JBC Papers in Press, October 10, 2007, DOI 10.1074/jbc.M705410200

Finn L. Aachmann[‡], Dmitri E. Fomenko[§], Alice Soragni[‡], Vadim N. Gladyshev[§], and Alexander Dikiy[‡1]

From the [‡]Department of Biotechnology, Norwegian University of Science and Technology, N-7491 Trondheim, Norway and the [§]Department of Biochemistry, University of Nebraska, Lincoln, Nebraska 68588

Selenium is a trace element with significant biomedical potential. It is essential in mammals due to its occurrence in several proteins in the form of selenocysteine (Sec). One of the most abundant mammalian Sec-containing proteins is selenoprotein W (SelW). This protein of unknown function has a broad expression pattern and contains a candidate C*XX*U (where U represents Sec) redox motif. Here, we report the solution structure of the Sec[13] → Cys variant of mouse SelW determined through high resolution NMR spectroscopy. The protein has a thioredoxin-like fold with the C*XX*U motif located in an exposed loop similarly to the redox-active site in thioredoxin. Protein dynamics studies revealed the rigidity of the protein backbone and mobility of two external loops and suggested a role of these loops in interaction with SelW partners. Molecular modeling of structures of other members of the Rdx family based on the SelW structure identified new conserved features in these proteins, including an aromatic cluster and interacting loops. Our previous study suggested an interaction between SelW and 14-3-3 proteins. In the present work, with the aid of NMR spectroscopy, we demonstrated specificity of this interaction and identified mobile loops in SelW as interacting surfaces. This finding suggests that 14-3-3 are redox-regulated proteins.

Many cellular processes are known to be regulated through reduction and oxidation (redox) (1). This regulation is carried out by a set of designated proteins, oxidoreductases. The redox function of these proteins may be supported by protein-bound cofactors or involve redox-active cysteine residues. Previous research on thiol oxidoreductases has focused only on a few of these enzymes (2). Most prominent among them are proteins of the thioredoxin fold superfamily, such as thioredoxin, glutaredoxin, peroxiredoxin, glutathione peroxidase, and their more distant homologs (3). Thiol oxidoreductases, however, are much more widespread, and most members of this protein class have not been functionally characterized (4).

In addition to oxidoreductases containing catalytic redox-active thiols, some enzymes evolved that possess an active site selenocysteine (Sec)[2] (5). Sec is known as the 21st amino acid in proteins (6). This rare amino acid is inserted into proteins contranslationally in response to a UGA codon. The human set of Sec-containing proteins (selenoproteomes) consists of 25 known members (7), and selenoproteomes have also been analyzed in a variety of other organisms. Several selenoproteins have recently been functionally characterized and found to be oxidoreductases (8). For example, both major cellular redox systems, the thioredoxin and glutathione systems, are dependent on selenoproteins (thioredoxin reductases and glutathione peroxidases, respectively). However, the functions of the majority of selenoproteins are not known.

We recently reported on a family of selenoproteins and their Cys homologs, designated as the Rdx family (9). Mammalian members of this family include selenoproteins SelW, SelT, SelH, SelV, and a Cys-containing Rdx12 protein. Functions are not known for any of these proteins. Through sequence analysis and structure modeling, we predicted that these proteins possess a thioredoxin-like fold, suggesting a redox nature of catalytic Sec residues.

Among Rdx proteins, the best characterized is SelW. It is a 9-kDa selenoprotein, abundant in muscle and brain (10–14). Expression of SelW is regulated by the availability of selenium in the diet. Native SelW was reported to occur in a complex with glutathione, which was attached to one of the Cys residues in the protein (10). Very little is known about SelT and Rdx12 (9), whereas recent studies revealed that SelH is a nucleolar protein that protects cells against stress associated with hydrogen peroxide (15). SelV is highly homologous to SelW but has an additional N-terminal proline-rich extension and is expressed specifically in testes (7).

By utilizing affinity columns containing mutant versions of Rdx proteins, we found that SelW binds 14-3-3 proteins, whereas Rdx12 binds glutathione peroxidase 1 (9). The functional importance of these interactions is not known. The SelW/14-3-3 interaction is particularly interesting, since the latter proteins are a class of abundant proteins with multiple cellular functions and roles in disease (16–19). In addition, the SelW/14-3-3 interaction differs from that observed for other 14-3-3 partners, since SelW does not have canonical 14-3-3 binding motifs (R(S/*X*)*X*pS*X*P or R*XXX*pS*X*P, where *X* denotes any amino acid residue, and pS represents a phospho-

* This research was supported by the faculty of Natural Sciences and Technology at the Norwegian University of Science and Technology and National Institutes of Health Grant GM061603. The costs of publication of this article were defrayed in part by the payment of page charges. This article must therefore be hereby marked "*advertisement*" in accordance with 18 U.S.C. Section 1734 solely to indicate this fact.

[S] The on-line version of this article (available at http://www.jbc.org) contains supplemental Fig. 1.

The atomic coordinates and structure factors (code 2NPB) have been deposited in the Protein Data Bank, Research Collaboratory for Structural Bioinformatics, Rutgers University, New Brunswick, NJ (http://www.rcsb.org/).

[1] To whom correspondence should be addressed. Tel.: 47735-97863; Fax: 47735-91283; E-mail: alex.dikiy@biotech.ntnu.no.

[2] The abbreviations used are: Sec, selenocysteine; NOE, nuclear Overhauser effect; NOESY, NOE spectroscopy.

rylated serine (20, 21). One possibility is that SelW regulates 14-3-3 in a redox manner; in the oxidized form (*e.g.* with a disulfide or a glutathionylated cysteine), 14-3-3 may be inactive and require a reduced form of SelW for activation. Determination of the three-dimensional structure of SelW as well as structural information on the SelW/14-3-3 interaction would be key in understanding both the structural basis and biological relevance of this interaction.

NMR spectroscopy is a powerful technique for structural characterization of proteins in solution as well as for monitoring interactions between two or more proteins. Additionally, NMR provides valuable information regarding mobility of various parts of the protein and its residues. Here, we used high resolution NMR spectroscopy to determine the structure of a founding member of the Rdx family, SelW, and examined its interactions with 14-3-3 proteins. These data revealed the thioredoxin-like fold in SelW and, therefore, other Rdx proteins and provided structural insights into the interaction of SelW with 14-3-3.

MATERIALS AND METHODS

Expression and Purification of SelW—Structural analysis was carried out with a recombinant bacterially expressed mouse SelW tagged at the C terminus with a His_6 tag and containing Cys in place of Sec^{13} and Ser in place of Cys^{10} (9). To uniformly label SelW with ^{15}N or $^{15}N/^{13}C$, cells were grown in M9 minimal medium containing 99% enriched $(^{15}NH_4)_2SO_4$ and 98% enriched $^{13}C_6$-labeled D-glucose (Spectra Stable Isotopes). His_6-SelW was overexpressed in *Escherichia coli* ER2566 (New England Biolabs) by growing cells at 37 °C until the $A_{600\ nm}$ reached 0.6, followed by induction of protein synthesis by the addition of 1 mM isopropyl 1-thio-β-D-galactopyranoside for 3 h. Cells were collected by centrifugation and disrupted by sonication in 25 mM phosphate buffer, pH 7.0, containing 10 mM NaCl and 0.05% Triton X-100 (Sigma). Additionally, 1 mM lysozyme (Sigma) and a half-tablet of Complete Protease Inhibitor mixture (Roche Applied Science) were added to the solution. Following centrifugation, supernatant was applied onto a TALON Co-IMAC-Sepharose column (BD Biosciences). The column was washed with 20 mM imidazole in 50 mM phosphate buffer, pH 7.0, 300 mM NaCl, followed by elution of protein with 200 mM imidazole in 50 mM phosphate buffer, pH 7.0, 300 mM NaCl buffer at 4 °C.

Expression and Purification of 14-3-3—14-3-3 expression plasmids included constructs that coded for N-terminal His-tagged 14-3-3γ (pQE30 with the gene Ywhag, kindly provided by Dr. A. Aitken) and C-terminal His-tagged 14-3-3β and 14-3-3γ (pTvHR21-SGC derived from YWHABA-c007 and YWHAGA-s001 clones, kindly provided by Dr. D. Doyle). The plasmids were transformed into *E. coli* ER2566 (New England Biolabs). Unlabeled 14-3-3 proteins were prepared by growing cells in LB medium. Different 14-3-3 forms were overexpressed by growing cells at 37 °C up to $A_{600\ nm}$ 0.6, followed by induction of protein synthesis with 1 mM isopropyl 1-thio-β-D-galactopyranoside for 4 h.

Cells containing N-terminal His-tagged 14-3-3γ were collected by centrifugation and disrupted using BugBuster® Master Mix (Novagen) containing Complete Protease Inhibitor mixture (Roche Applied Science). Following centrifugation, the supernatant was applied onto an Ni^{2+}-nitrilotriacetic acid His-Bind resin column (Novagen). The column was washed with 20 mM imidazole in 50 mM phosphate buffer, pH 7.0, 300 mM NaCl buffer, followed by protein elution with 200 mM imidazole in WEB buffer at 4 °C.

Cells expressing C-terminal tagged 14-3-3β/γ were harvested by centrifugation; disrupted by sonication in 50 mM HEPES buffer, pH 8.0, containing 500 mM NaCl, 5 mM imidazole, and 5% glycerol (Sigma); and supplemented with 1 mM lysozyme (Sigma) and Complete protease inhibitor mixture (Roche Applied Science). Cell lysate was applied onto a Ni^{2+}-nitrilotriacetic acid His-Bind resin column (Novagen). The column was washed with 25 mM imidazole in 50 mM HEPES buffer, pH 8.0, containing 500 mM NaCl and 5% glycerol, followed by elution of protein with 250 mM imidazole in 50 mM HEPES buffer, pH 8.0, containing 500 mM NaCl at 4 °C.

Sample Preparation—Samples for NMR studies contained 1–1.5 mM His_6-SelW in 25 mM phosphate buffer, pH 5.1, with 50 mM NaCl, 2.5 mM dithiothreitol in the presence of either 95% H_2O plus 5% D_2O or 99.9% D_2O.

Interaction of SelW with 14-3-3—Interaction between SelW and 14-3-3 was investigated by mixing 0.2–0.5 mM ^{15}N-labeled SelW with unlabeled 14-3-3 at a molar ratio of 1:1.1 (SelW/14-3-3]) in 25 mM phosphate buffer, pH 6.0, containing 150 mM NaCl. ^{15}N HSQC spectra were recorded, and the spectral changes were quantified as $\Delta_{HSQC} = |\Delta\upsilon_{HN}|$. As control, bovine serum albumin (Sigma) was mixed with ^{15}N-labeled SelW as described above for 14-3-3, and the spectra were recorded.

NMR Spectroscopy—All NMR experiments were recorded at 288 or 298 K on a Bruker DRX600 spectrometer equipped with a 5-mm *z*-gradient T*X*I(H/C/N) cryogenic probe. ^1H, ^{13}C, and ^{15}N, chemical shifts were referenced to sodium salt of 3-(trimethylsilyl)propanesulfonic acid as described in Ref. 22. Sequence-specific backbone and side-chain assignments of SelW were accomplished using ^{15}N HSQC, ^{13}C HSQC, HNCA, HN(CO)CA, HNCO, HN(CA)CO, CBCANH, CBCA(CO)NH, HBHANH, HBHA(CO)NH, HCCH-TOCSY, and HCCH-COSY spectra. Aromatic ring system assignments were obtained from two-dimensional COSY, TOCSY, and NOESY experiments. NOE assignments were derived from two-dimensional NOESY, three-dimensional ^1H-^{15}N HSQC-NOESY and ^1H-^{13}C HSQC-NOESY spectra. Dihedral angle constraints were derived from three-dimensional HNHA spectra. NMR data were processed with the BRUKER XWinNMR version 3.5 software, and spectral analysis was performed using CARA version 1.4 (23). ^{15}N-{^1H} heteronuclear NOEs were calculated from two independently measured and integrated ^{15}N-^1H heteronuclear correlated spectra acquired using enhanced sensitivity sequence employing pulsed field gradients (24) as the ratio of the volumes with and without ^1H saturation. Nuclear magnetic relaxation (T_1 and T_2) measurements of ^{15}N were obtained by exponential fitting of peak intensities in ^{15}N HSQC spectra acquired with different relaxation delays (24, 25). All NMR data reported in this work were collected at the faculty of Natural Sciences and Technology, Norwegian University of Science and Technology NMR center.

TABLE 1

Characterization of input NMR data and structural statistics for the solution structure of the reduced recombinant Sec^{13} → Cys form of mouse SelW

Parameters	Values
Input data for structure calculation	
NOE distance constraints	
Total	1950
Intra	1063
Short	341
Medium	236
Long	310
Torsion angle constraints	116
Structure statistics, 20 conformers[a]	
CYANA target function value(Å^2)	3.53 ± 0.26
Maximum residual distance constraint violation (Å)	0.4 ± 0.13
Maximal torsion angle constraint violations	2.75 ± 0.75
Total AMBER energies (kcal·mol^{-1})	−1304.2 ± 292.7
PROCHECK Ramachandran plot analysis	
Residues in favored regions (%)	81.6
Residues in additionally allowed regions (%)	16.3
Residues in generously allowed regions (%)	1.4
Residues in disallowed regions (%)	0.8
Root mean square deviation to the average coordinates (Å)[b]	
N, C$^\alpha$, C′ (residues 3–88)	0.71 ± 0.12
N, C$^\alpha$, C′ (secondary structure)[c]	0.41 ± 0.10
Heavy atoms (residues 3–88)	1.12 ± 0.11
Heavy atoms (secondary structure)[c]	0.86 ± 0.10

[a] The values given are the average and S.D. over the 20 energy-minimized conformers with the lowest CYANA (version 2.1.5) target function values that represent the NMR solution family.
[b] Concerns energy-minimized conformers.
[c] Residues 3–9, 15–28, 34–40, 48–63, 70–88.

Structure Calculation—NOE cross-peaks were identified, integrated, and assigned in the aforementioned NOESY spectra using the program CARA (23). The CALIBA (26) subroutine in CYANA 2.1 was used to convert cross-peak intensities from NOESY spectra into distance constraints. Dihedral angle constraints were derived from three-dimensional HNHA spectra and were further confirmed and supplemented with backbone torsion angle restraints obtained from secondary chemical shifts using the TALOS program (27). On the basis of this input, the structure was calculated using the torsion angle dynamics program CYANA 2.1 (28). Structure calculations started from 96 conformers with random torsion angle values, and the final 20 conformers with the lowest final CYANA target function values were energy-minimized in a vacuum using the AMBER force field (29) with the aid of the AMBER 9.0 program.

Modeling of Rdx Proteins—Structures of mouse Rdx12 and SelT were modeled using Modeler8 version 2 based on the experimental NMR structure of mouse SelW.

RESULTS AND DISCUSSION

General Description of the SelW Structure—Assignment of ^{1}H, ^{15}N, and ^{13}C resonances for a recombinant C10S and U13C variant of mouse SelW (hereafter SelW) was achieved through standard two- and three-dimensional homo-/heteronuclear NMR experiments. The resonance assignment was confirmed at two temperatures, 288 and 298 K. A list of NMR experiments that resulted in the assignment together with the assignment itself were deposited in the Biological Magnetic Resonance Bank under accession number 7324. Geometrical constraints were derived from two-dimensional homonuclear and three-dimensional heteronuclear ^{15}N- and ^{13}C-edited NOESY. Table 1 reports distribution of constraints among four different classes according to the types of constraints and distances. Dihedral angle constraints were derived from three-dimensional HNHA spectra and were further confirmed and supplemented using the TALOS program (27). In total, 1950 NOE upper distance limit constraints and 116 angle restraints were used to calculate the three-dimensional structure of SelW using the CYANA 2.1 program, assuring high quality of the calculated structure. The structures constituting the CYANA family were further subjected to refinement using the AMBER 9.0 program (29). The coordinates of the final energy-refined family (20 conformers) together with the constraint files were deposited in the Protein Data Bank under accession code 2NPB.

Fig. 1 shows a family of 20 conformers (*A*) and different orientations of the average three-dimensional structure (*B* and *C*) of SelW. Quality assessment for the calculated structure is reported in Table 1. The data suggest that the resulting SelW structure represents a low energy conformation with the structural data fitting well the experimentally found geometrical constraints.

The observed structural family is well defined. Average backbone root mean square deviation value with respect to the mean structure is 0.71 ± 0.12 Å. If only the protein regions characterized by the presence of secondary structure are considered, the corresponding root mean square deviation value drops to 0.41 ± 0.10 Å. Indeed, the least defined regions in the SelW family are located in two external loops (Fig. 1*A*). Decreased resolution for these regions is due to a decreased number of geometrical constraints for residues constituting the two loops. One of the loops contains a predicted active site of SelW (*e.g.* the C*XX*U motif), whereas the second loop may be involved in substrate binding (see below). The decreased structural resolution observed for the two loops may be a consequence of increased mobility of these regions with respect to the rest of the protein. Moreover, the proposed mobility may have a physiological role (*i.e.* it may be required for induced fit binding between interacting partners). To examine this possibility, dynamic characterization of the protein by NMR spectroscopy was carried out (see below).

The structure of SelW consists of a four-stranded β-sheet with two extended α helices and a short 3^{10} helix, all located on one side of the β-sheet (Fig. 1, *B* and *C*). Besides these secondary structures, the protein contains two external loops and a type II turn. The molecule is characterized by a β_1(3–9)-α_1(15–28)-β_2(34–40)-β_3(48–52)-β_4(54–60)-3^{10}(61–63)-α_2(70–88) secondary structure pattern, wherein β_1 and β_2 are parallel strands forming a classical β_1-α_1-β_2 motif, which is also observed in thioredoxin-like fold proteins (30). The axis of α_2-helix is at an ~45° angle with respect to the axis of the α_1-helix as a consequence of the β-sheet topology. The C*XX*U motif is located in the loop (residues 10–14) between β_1 and α_1. The second loop (residues 40–47) separates β_2 and β_3 strands. β_3 and β_4 strands form a β-hairpin with a type II turn (residues 52–54) in between. In the β_4 strand, Val^{57} is flipped out as previously observed for Val^{56} in tendamistat (31).

Electrostatic Surface Potential—The electrostatic surface potential of mouse SelW is shown in Fig. 1*D*. The data reveal that electrostatic charges are rather smoothly distributed over the protein surface. Indeed, the surface lacks strong positive or

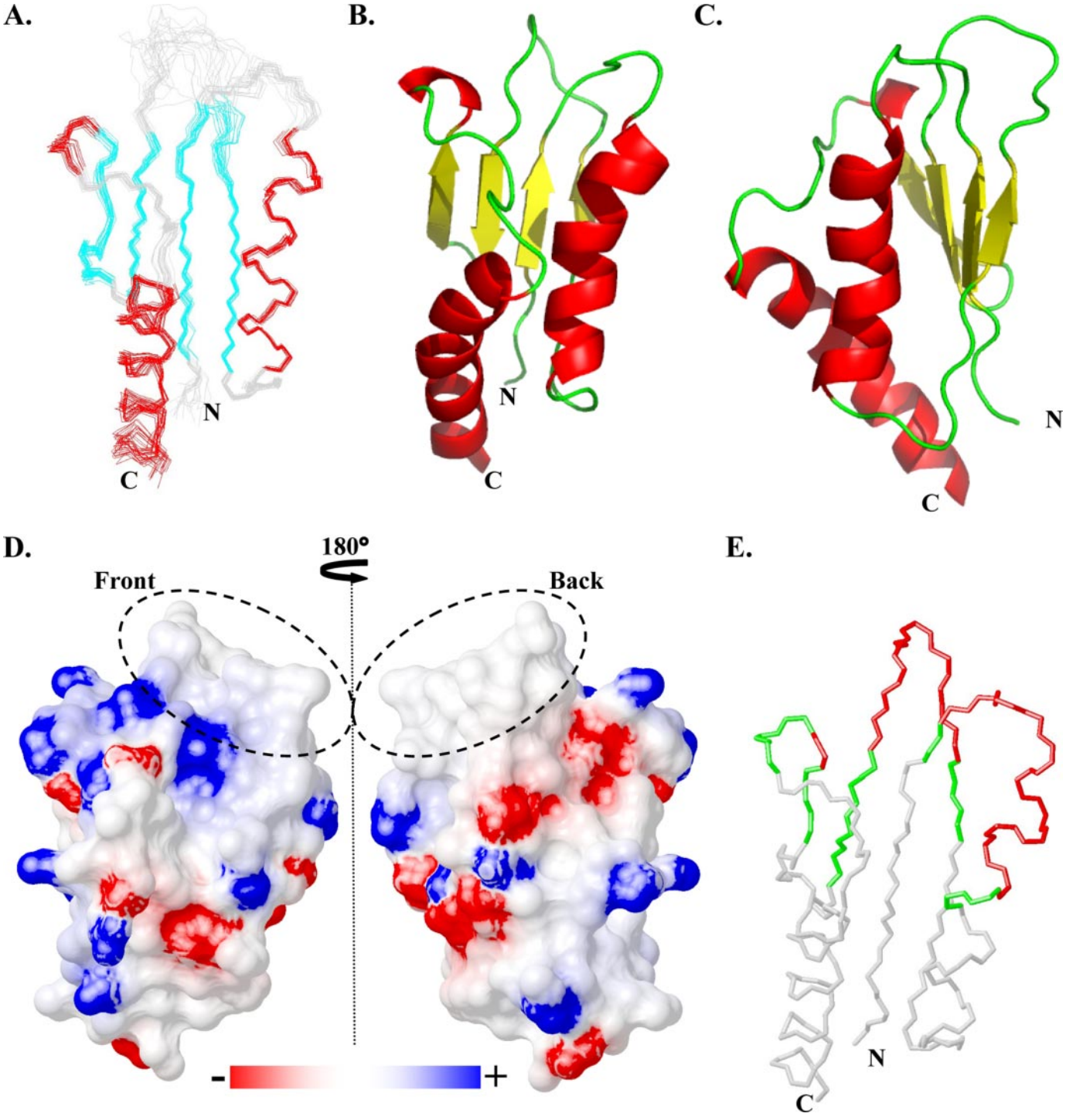

FIGURE 1. **Three-dimensional energy-minimized solution structure of reduced recombinant mouse SelW.** *A*, SelW structural family consisting of 20 conformers with lowest target function; *B* and *C*, two different orientations of the family mean structure showing secondary structure of the protein; *D*, two orientations of the protein surface electrostatic potential related by 180° rotation along the *vertical axis*. External loops of the protein are *circled*; *E*, backbone structure of the protein, in which regions involved in the interaction with 14-3-3 are *colored* as follows: *gray*, residues that either changed their amidic proton chemical shift by less than |5| Hz or remained unchanged; *green*, residues for which analogous chemical shift changes were more than |5| Hz; *red*, residues for which cross-peaks were broadened beyond detection, and the corresponding cross-peaks were not detected in the ^{15}N HSQC spectrum. Structural models were prepared using MOLMOL (35) and PyMOL (36) programs.

negative patches. Nevertheless, a small positively charged region is found in the 3^{10} helix (residues 61–63). Both external loops (Tyr^{9}-Ser^{10}-Gly^{11}-Ala^{12}-Cys^{13}-Gly^{14}-Tyr^{15} and Glu^{39}-Gly^{40}-Thr^{41}-Pro^{42}-Asn^{43}-Val^{44}-Thr^{45}-Gly^{46}-Phe^{47}) (indicated by *circles* in Fig. 1*D*) lack charged amino acids (with the possible exception of Cys in the C*XX*U motif). This observation suggests that the interaction between SelW and its physiological partner(s) takes place without the assistance of electrostatic forces. Moreover, it should be noted that three of the four loop ends contain aromatic amino acids. They might work as anchoring

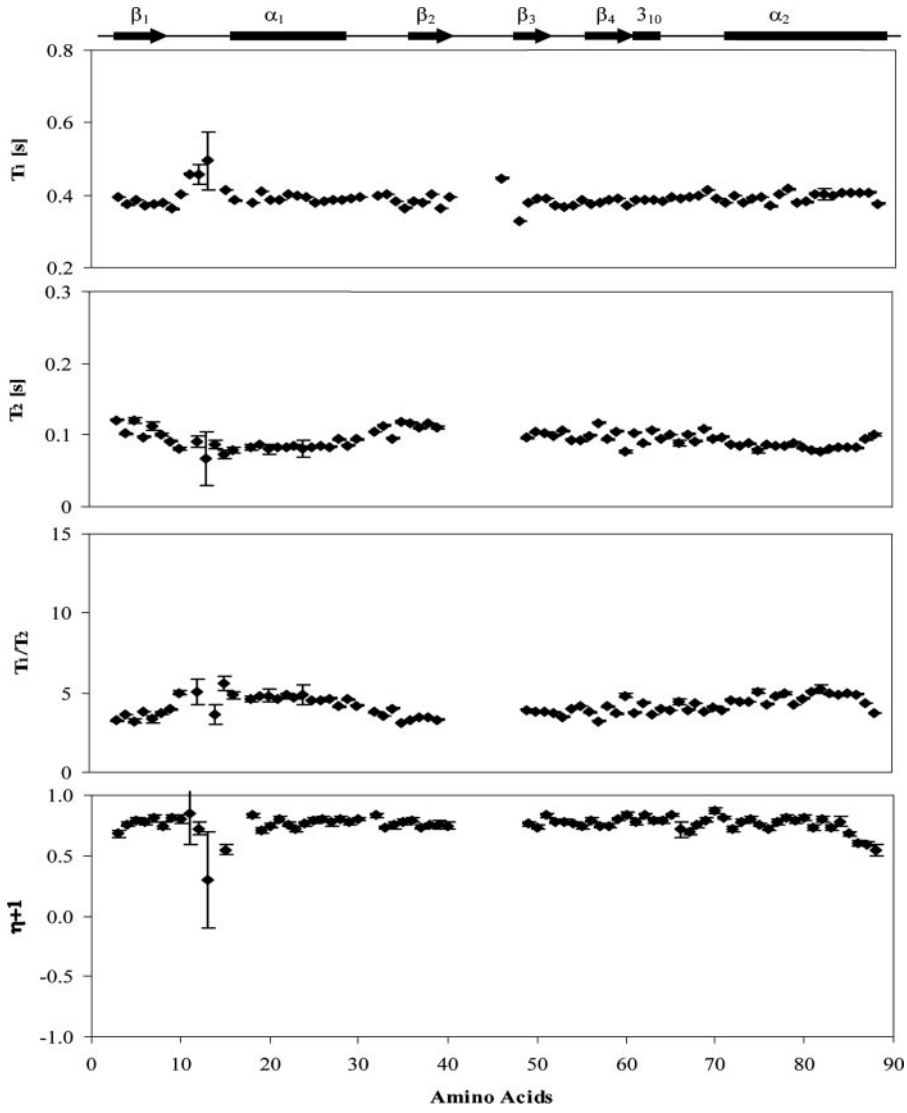

FIGURE 2. **^{15}N relaxation data and ^{15}N-{^{1}H} heteronuclear NOE for reduced SelW.** The *error bars* indicate S.D. determined from replicate measurements. Secondary structure elements of the protein are reported at the *top*.

points for the loops in relation to the protein backbone core. Furthermore, these residues are often flanked by glycines (*i.e.* Gly^{14}, Gly^{40}, and Gly^{46}) and a serine (Ser^{10}), which might offer greater backbone flexibility and support loop mobility. Altogether, these residues may confer both rigidity to the structural elements and increased flexibility to the loops, resulting in an optimal structural network for the predicted catalytic site of SelW.

Mobility Studies—As discussed above, the two external loops in the solution structure of SelW reveal a markedly lower resolution with respect to the rest of the protein that could be explained by increased loop mobility. To examine this possibility, we elucidated dynamic behavior of SelW in a ps/ns time scale through analysis of ^{15}N backbone T_1 and T_2 and heteronuclear ^{15}N-{^{1}H} NOE values. Fig. 2 reports these parameters as a function of residue number. It is evident that the vast majority of residues exhibit T_1, T_2, and NOE values characteristic of nonmobile amino acids in a protein of the SelW size. However, the data cannot sufficiently describe the residues of the two external loops (*i.e.* residues 10–14 and 40–47). Intensities of the corresponding cross-peaks in ^{15}N HSQC spectra are significantly lower with respect to those of other residues; therefore, the errors for relaxation times and heteronuclear NOEs are significantly higher. The significantly decreased intensity of the relevant cross-peaks in ^{15}N HSQC spectra suggests that the loop residues are more mobile than the rest of the molecule. For the rigid part of SelW, the T_1/T_2 ratio was 4.37, which, assuming a spherical geometry of the particle, corresponds to an overall rotational correlation time $\tau_c = 5.8$ ns (25).

Structural Comparison of Mouse and Bacterial SelW Proteins—During the course of this study, an unpublished crystal structure of a distant bacterial SelW homolog appeared in the Protein Data Bank (accession code 2FA8). Structural comparison of mammalian and bacterial proteins is important from both functional and evolutionary points of view. Structure-assisted alignment of these two sequences (*i.e.* Protein Data Bank codes 2NPB and 2FA8) shows 18.2% identity in amino acid sequences. Interestingly, in pairwise alignments, BLAST and FASTA do not recognize these proteins as homologs with sufficient *E* values. Nevertheless, mouse SelW and bacterial SelW-like proteins show an overall conservation of both structure and the predicted active site C*XX*C/U motif. These proteins also conserve the β-hairpin (residues 48–56 in mouse SelW) as well as positively charged residues in the 3^{10} helix. Side-by-side views of mouse and bacterial SelW structures are shown in Fig. 3 (this analysis was performed using the coordinates of one bacterial SelW monomer in the crystal structure of the tetramer). The calculated backbone root mean square deviation value was 1.43 Å, indicating very similar three-dimensional structures in mammalian and bacterial SelWs. In turn, close structural similarity suggests that the proteins may exhibit similar functions in bacteria and mammals.

Fig. 3*A* shows the side chains of all aromatic residues in the mouse SelW structure. Of eight aromatic residues, six (9, 15, 19, 47, 48, and 66) form a cluster right behind the predicted active site of SelW. This cluster is situated too far from the C*XX*C(U) motif (average distance is ~15 Å) to have a direct role in the redox reaction. However, it might be relevant for binding of interaction partners and/or maintaining the overall protein structure. This possibility is consistent with the strict conser-

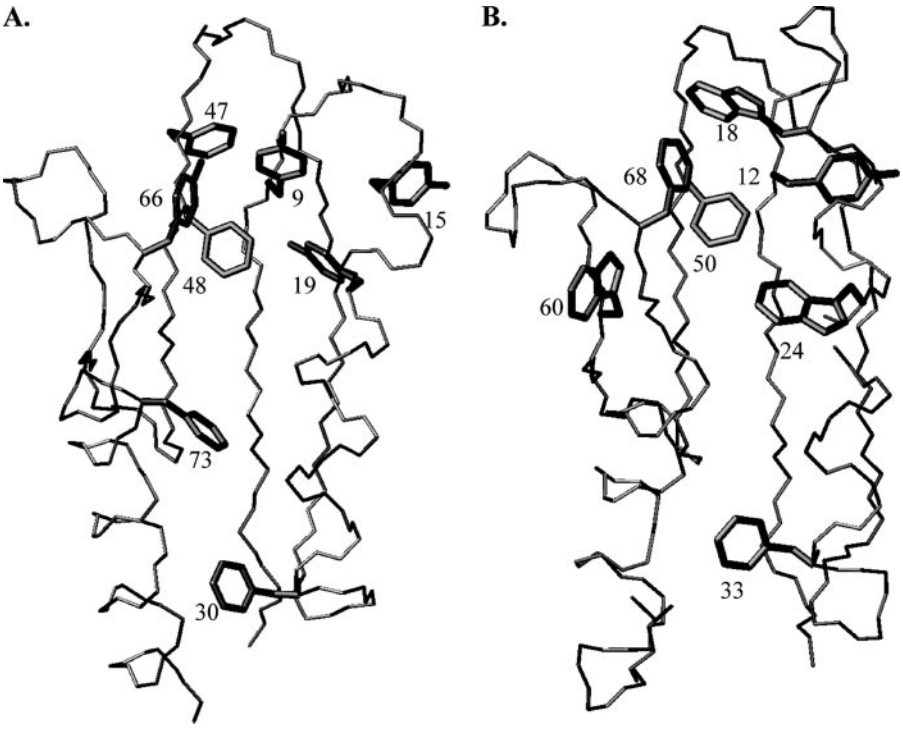

FIGURE 3. **Backbone structure of reduced SelW that shows aromatic amino acid side chains.** *Numbering* corresponds to the indicated aromatic amino acids. *A*, mouse SelW (Protein Data Bank code 2NPB); *B*, bacterial SelW-like homolog (Protein Data Bank code 2FA8).

vation of all aromatic residues in the "aromatic cluster" (see also below) upon comparison of mouse (Fig. 3*A*) and bacterial (Fig. 3*B*) SelW structures.

Structural Characterization of Other Rdx Family Members—The three-dimensional structure of SelW allowed us to model structures of other members of the Rdx family. Fig. 4*A* shows SelT, Rdx12, and SelW structures, together with the structure of reduced thioredoxin (for comparison). The four proteins contain several common structural elements, including the overall β-α-β-β-β-α secondary structure core. However, in thioredoxin, an additional α-helix is inserted between the second and third β strands. This helix is part of the overall thioredoxin fold. Thus, Rdx family proteins possess a thioredoxin-like fold as recently defined (30).

The Rdx12 structural model is similar to the structure of SelW, with the exception that Rdx12 has a 24-amino acid N-terminal extension upstream of the β_1 strand as well as 9 amino acids downstream of α_2-helix. The secondary structure of Rdx12, $\beta_1(25–28)$-$\alpha_1(35–49)$-$\beta_2(53–56)$-$\beta_3(65–69)$-$\beta_4(72–76)$-$3^{10}(77–79)$ and $\alpha_2(87–105)$, closely mimics that of SelW. β strands in the β_1-α_1-β_2 motif appear to be shorter in Rdx12 than in SelW, and its α_2-helix is positioned such that it covers the N-terminal upper part of the protein.

The SelT model includes $\beta_1(1–3)$-$\alpha_1(9–23)$-$\beta_2(29–32)$-$\beta_3(36–40)$-$\beta_4(43–47)$-$3^{10}(48–51)$-$\alpha_2(58–76)$ secondary structure pattern. The N-terminal part begins with the β_1 strand, resulting in shorter β strands in the β_1-α_1-β_2 motif with respect to SelW. Additionally, SelT contains a 70-amino acid insertion consisting of four predicted helices between β2 and β3 strands. The function of this insert is not known, but it is located in the modeled structure near the C*XX*U motif.

Our structural analysis shows that the predicted active sites of SelW, Rdx12, and SelT are located in the first external loop between β1 and α1 elements. Besides this feature, another common structural element in all Rdx proteins is the aromatic cluster behind the active center, suggesting a common function of this cluster in these proteins. Additionally, two external loops in this class of proteins lack charged residues.

Structural Comparison of the Rdx Family and Structurally Related Sec-containing Proteins—Recently, the structures of Cys versions of two thioredoxin-like selenoproteins, Sep15 and SelM (Fig. 4*B*), were determined (32) (Protein Data Bank codes 2A4H and 2A2P, respectively). These proteins are structurally related to Rdx proteins in having an overall thioredoxin-like fold and lacking the thioredoxin helix following the β_1-α_1-β_2 structural motif. The second loop appears to be shorter in Sep15 and SelM, similar to that in the Rdx family. One difference between Rdx proteins on one side and Sep15 and SelM on the other is that the α_1-helix in the latter proteins is divided into two smaller α-helices with a kink in between.

All proteins shown in Fig. 4 lack charged and hydrophobic residues within the two external loops, which appears to be a characteristic feature of these proteins. On the other hand, thioredoxin, Sep15, and SelM, in contrast to Rdx proteins, do not have the aromatic cluster. Since the fold of all of these proteins is roughly the same, we can exclude the role of aromatic residues in maintaining protein topology.

Interaction between SelW and 14-3-3—Our previous studies revealed that 14-3-3 proteins bind SelW in pull-down and immunoprecipitation experiments (9). To characterize the structural basis of this interaction, we examined binding between these two proteins by NMR spectroscopy. The interaction between SelW and 14-3-3 was monitored through spectral changes in ^{15}N HSQC spectra of labeled SelW upon the addition of unlabeled 14-3-3. This way, the changes occurring with the heteronuclear ^{1}H-^{15}N spectrum of SelW were not hampered by additional peaks arising from 14-3-3 and could be reliably deciphered.

β and γ forms of 14-3-3 were investigated as both N- and C-terminal His-tagged proteins. Interestingly, although 14-3-3 containing a C-terminal His tag was folded, the same protein containing an N-terminal His tag was not and, therefore, was not suitable for structural studies. Consistent with this observation, the ^{15}N HSQC spectrum of SelW was not changed upon the addition of the N-terminally tagged 14-3-3γ, indicating that the unfolded 14-3-3 does not interact with SelW.

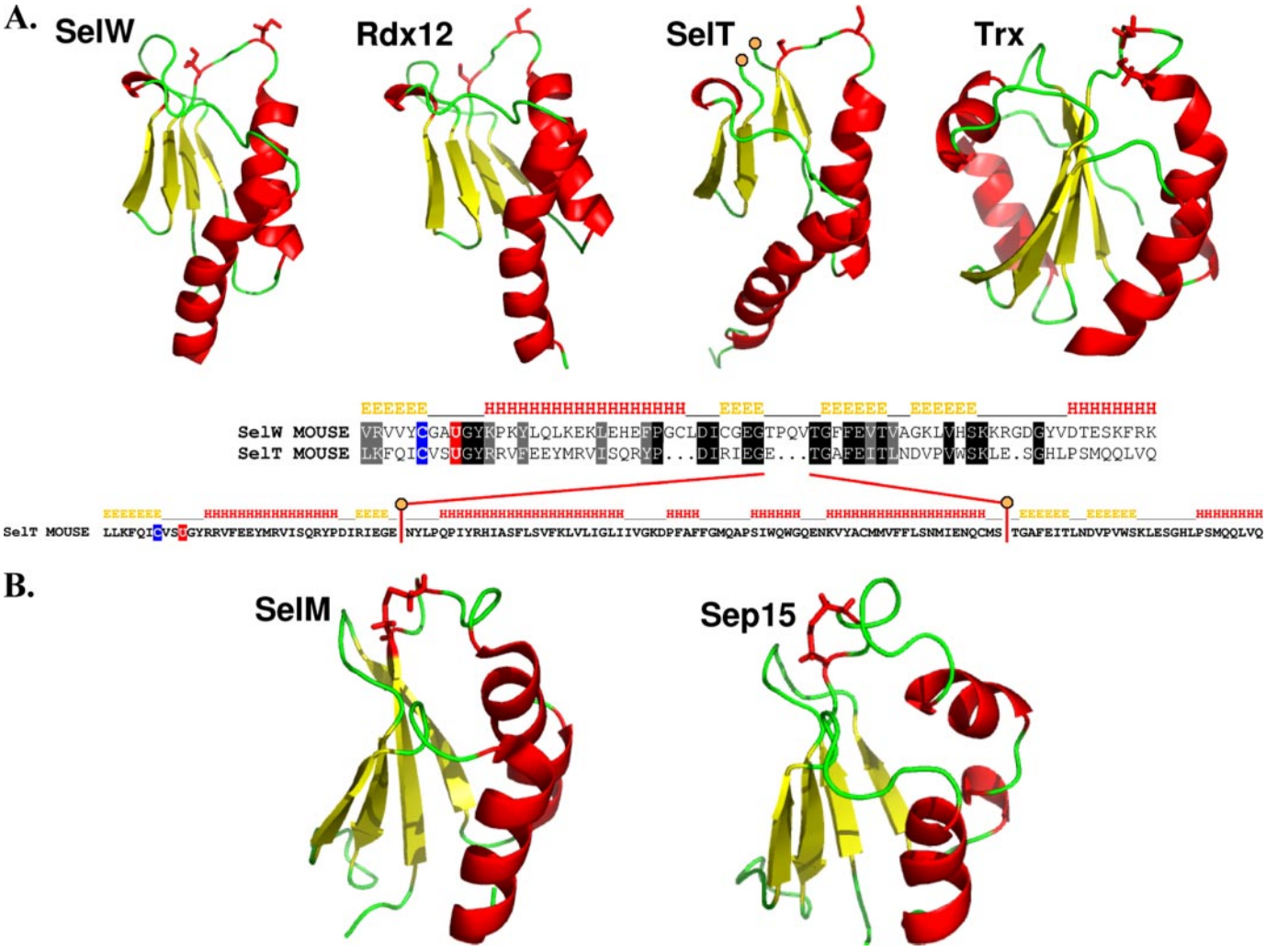

FIGURE 4. **Comparison of three-dimensional structures of SelW, Rdx family members, and thioredoxin.** Secondary structure elements are shown for each protein. Predicted redox-active cysteines (or Sec) are *highlighted* in *red*. *A*, backbone structural models of proteins constituting the Rdx family: SelW, Rdx12, and SelT. For comparison purposes, the backbone structure of human thioredoxin (Protein Data Bank code 3TRX) is also shown. N- and C-terminal extensions within the Rdx12 structural model are not shown. The SelT model contains a gap that corresponds to an α-helix region insert as shown in the alignment in the figure. Gap ends are marked by *orange circles*. Sequences were aligned with ClustalW and shaded with BoxShade3.21. *B*, three-dimensional solution structures of SelM (Protein Data Bank code 2A2P) and Sep15 (Protein Data Bank code 2A4H). N- and C-terminal extensions in both proteins are not shown.

In contrast, the addition of either β or γ forms of 14-3-3 containing C-terminal His tags to the labeled SelW resulted in the same significant changes in the SelW heteronuclear spectrum. ^{15}N HSQC spectra of SelW alone and SelW in the presence of the 14-3-3γ isoform (molar ratio 1:1.1) are shown in Fig. 5 (*A* and *B*). A simple visual comparison shows that although the general pattern of ^{15}N HSQC SelW spectra in both cases remained the same, the spectra bear significant differences. Some cross-peaks disappeared from the ^{15}N HSQC SelW spectrum upon the addition of 14-3-3 (significant increase in the signal line widths), and other peaks shifted, whereas the positions of the majority of the cross-peaks remained unchanged. Such changes in the NMR spectra are indicative of interaction occurring between these proteins. Our results, therefore, confirm previous data (9) on the interaction between 14-3-3 and SelW.

The fact that SelW does not interact with the unfolded N-terminally tagged 14-3-3 indicates that the observed interaction between SelW and 14-3-3 is specific. To further examine this interaction, we monitored changes occurring in ^{15}N HSQC SelW spectrum upon the addition of bovine serum albumin. The latter is a 66.4-kDa protein and therefore has a size comparable with that of 14-3-3 (homodimer is a 56-kDa protein). Supplemental Fig. 1 shows the ^{15}N HSQC spectrum of SelW in the presence of bovine serum albumin at a molar ratio of 1:1.1 (SelW/bovine serum albumin). Comparison of this spectrum with that of SelW alone (Fig. 5*A*) identified no differences, indicating that these two proteins do not interact in solution. Overall, our data strongly suggest that the SelW-14-3-3 interaction is both specific and probably physiologically relevant.

Taking advantage of the SelW NMR assignment, we also determined the identity of SelW residues that are involved in this interaction by comparing chemical shifts of the corresponding nuclei in respective spectra (*i.e.* reference spectrum *versus* the spectrum following the addition of the target compound). Residues whose nuclei show either change in chemical shift or broadening of NMR signals are involved in the interaction between two molecules, whereas other residues, for which

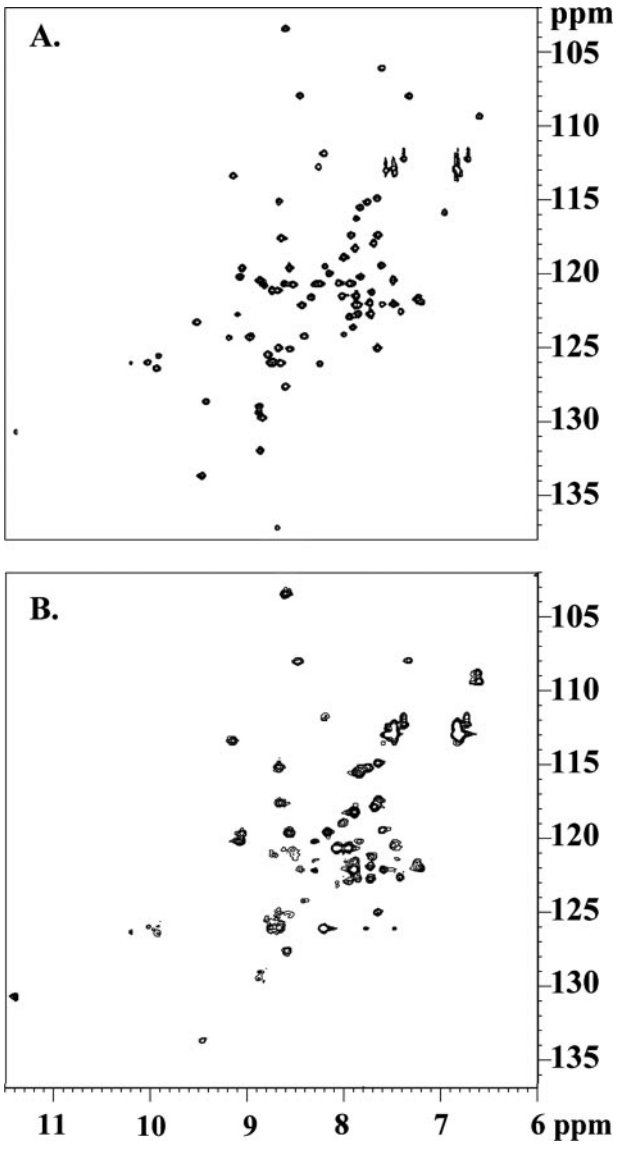

FIGURE 5. **Two-dimensional ^{15}N HSQC spectra of reduced SelW in the presence and absence of 14-3-3 at 298 K.** *A*, SelW (reference spectrum); *B*, SelW in the presence of recombinant 14-3-3γ (molar ratio 1:1.1).

no spectral changes are observed, are neither coupled to nor directly involved in it (33, 34). In our work, both shifts of cross-peaks and broadening of NMR signals beyond detection were observed upon the addition of γ-14-3-3 to SelW. Fig. 6 shows chemical shift differences for the corresponding amidic proton nuclei as a function of residue number. The chemical shift difference for residues whose cross-peaks in the ^{15}N HSQC spectrum broadened beyond detection and which, therefore, were located at the interacting interphase, was attributed to |50| Hz (a maximal value reported in Fig. 6) for visualization purposes. The analogous behavior was also observed for β-14-3-3. As can be seen in Fig. 6, SelW contains three regions characterized by perturbation of NMR properties of amino acids (*i.e.* involved in the interaction with 14-3-3): residues 8–22, 38–51, and 58–64. These regions are mapped on the SelW structure and *differently colored* in Fig. 1*E*. Our data demonstrate that two external loops (residues 9–15 and 40–48) and a short 3^{10} turn (residues 60–63) of SelW are involved in binding of 14-3-3.

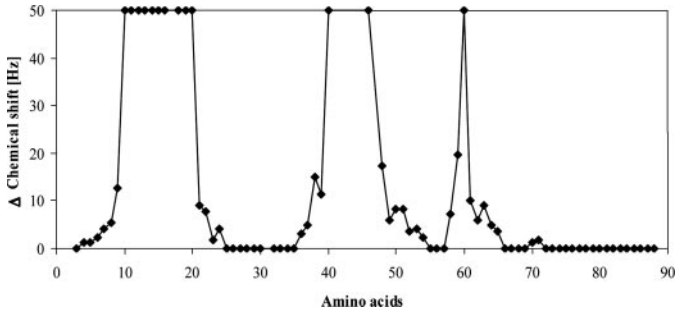

FIGURE 6. **Difference in amidic proton NMR chemical shifts as a function of residue number between reduced recombinant mouse SelW and the same protein in the presence of recombinant 14-3-3γ (molar ratio 1:1.1).** For the residues for which cross-peaks in ^{15}N HSQC spectrum disappear upon the addition of 14-3-3γ, the difference was ascribed for visualization purposes to |50| Hz. The residues for which no data are reported in the figure are either prolines or those for which the corresponding ^{1}H-^{15}N cross-peaks were not detected in the reference ^{15}N HSQC spectrum of reduced SelW.

We hypothesize that the proposed increased mobility of these loops is functionally relevant and is required for interaction of SelW with its physiological partners. Our results complement those previously reported regarding this interaction through biochemical studies (9). Taken together, it appears that SelW and 14-3-3 proteins interact in solution via the formation of an intermolecular complex. Having the thioredoxin-like fold and C*XX*C(U) motif in SelW, such interaction could be redox-sensitive. The most plausible scenario for this reaction would involve intermolecular reduction of the oxidized 14-3-3 protein by SelW. Cys^{13} (the residue that replaces the natural Sec^{13}) is located in the first external loop and might play the role of the attacking residue in the reduction reaction, whereas Cys^{10} may be a resolving residue. The exact mechanism of the interaction between SelW and 14-3-3 should await determination of the structure of the intermolecular complex, in progress in our laboratories.

Conclusions—In conclusion, this study reports the first solution structure of mammalian SelW that was calculated through high resolution NMR spectroscopy. The structure revealed a thioredoxin-like fold, a β-α-β-β-β-α secondary structure core, and a C*XX*U (S*XX*C in the mutant) motif in an exposed loop in a position similar to the redox-active C*XX*C site in thioredoxin.

The SelW structure permitted interpretation of the sequences of homologous proteins and prediction of their structures. The NMR-derived structure also suggested a role for SelW in redox regulation. Analysis of protein dynamics revealed rigidity of the backbone except for two external loops. These loops appear to participate in the interaction of SelW with 14-3-3 proteins. A specific interaction with folded 14-3-3 protein was found to involve the conserved active site C*XX*U residues, suggesting that the interaction could depend on the redox state of SelW.

Acknowledgments—We thank Dr. A. Aitken (University of Edinburgh, Scotland) for providing an expression construct for the N-terminal His-tagged 14-3-3γ and Dr. D. Doyle (University of Oxford) for the C-terminal His-tagged 14-3-3 β/γ proteins. We are grateful to Dr. Reinhard Wimmer (Aalborg University, Denmark) for help with TALOS and CYANA software.

REFERENCES

1. Halliwell, B. (2006) *Plant Physiol.* **141,** 312–322
2. Lillig, C. H. (2007) *Antioxid. Redox Signal.* **9,** 25–47
3. Martin, J. L. (1995) *Structure* **3,** 245–250
4. Fomenko, D. E., Xing, W., Adair, B. M., Thomas, D. J., and Gladyshev, V. N. (2007) *Science* **315,** 387–389
5. Stadtman, T. C. (1996) *Annu. Rev. Biochem.* **65,** 83–100
6. Hatfield, D. L., Berry, M., and Gladyshev, V. N. (2006) *Selenium: Its Molecular Biology and Role in Human Health*, Springer-Verlag New York Inc., New York
7. Kryukov, G. V., Castellano, S., Novoselov, S. V., Lobanov, A. V., Zehtab, O., Guigo, R., and Gladyshev, V. N. (2003) *Science* **300,** 1439–1443
8. Flohe, L. (2005) *Dev. Ophthalmol.* **38,** 89–102
9. Dikiy, A., Novoselov, S. V., Fomenko, D. E., Sengupta, A., Carlson, B. A., Cerny, R. L., Ginalski, K., Grishin, N. V., Hatfield, D. L., and Gladyshev, V. N. (2007) *Biochemistry* **46,** 6871–6882
10. Beilstein, M. A., Vendeland, S. C., Barofsky, E., Jensen, O. N., and Whanger, P. D. (1996) *J. Inorg. Biochem.* **61,** 117–124
11. Vendeland, S. C., Beilstein, M. A., Chen, C. L., Jensen, O. N., Barofsky, E., and Whanger, P. D. (1993) *J. Biol. Chem.* **268,** 17103–17107
12. Gu, Q. P., Sun, Y., Ream, L. W., and Whanger, P. D. (2000) *Mol. Cell Biochem.* **204,** 49–56
13. Sun, Y., Gu, Q. P., and Whanger, P. D. (2001) *J. Inorg. Biochem.* **84,** 151–156
14. Loflin, J., Lopez, N., Whanger, P. D., and Kioussi, C. (2006) *J. Inorg. Biochem.* **100,** 1679–1684
15. Novoselov, S. V., Kryukov, G. V., Xu, X. M., Carlson, B. A., Hatfield, D. L., and Gladyshev, V. N. (2007) *J. Biol. Chem.* **282,** 11960–11968
16. Yaffe, M. B. (2002) *FEBS Lett.* **513,** 53–57
17. van Heusden, G. P. H. (2005) *IUBMB Life* **57,** 623–629
18. Darling, D. L., Yingling, J., and Wynshaw-Boris, A. (2005) *Curr. Top. Dev. Biol.* **68,** 281–315
19. Pozuelo Rubio, M., Geraghty, K. M., Wong, B. H., Wood, N. T., Campbell, D. G., Morrice, N., and Mackintosh, C. (2004) *Biochem. J.* **379,** 395–408
20. Yaffe, M. B., Rittinger, K., Volinia, S., Caron, P. R., Aitken, A., Leffers, H., Gamblin, S. J., Smerdon, S. J., and Cantley, L. C. (1997) *Cell* **91,** 961–971
21. Rittinger, K., Budman, J., Xu, J., Volinia, S., Cantley, L. C., Smerdon, S. J., Gamblin, S. J., and Yaffe, M. B. (1999) *Mol. Cell* **4,** 153–166
22. Zhang, H. Y., Neal, S., and Wishart, D. S. (2003) *J. Biomol. NMR* **25,** 173–195
23. Keller, R. (2004) *Optimizing the Process of Nuclear Magnetic Resonance Spectrum Analysis and Computer Aided Resonance Assignment.* Ph.D. thesis, Swiss Federal Institute of Technology, Zurich, Switzerland
24. Farrow, N. A., Muhandiram, R., Singer, A. U., Pascal, S. M., Kay, C. M., Gish, G., Shoelson, S. E., Pawson, T., Forman-Kay, J. D., and Kay, L. E. (1994) *Biochemistry* **33,** 5984–6003
25. Kay, L. E., Torchia, D. A., and Bax, A. (1989) *Biochemistry* **28,** 8972–8979
26. Güntert, P., Qian, Y. Q., Otting, G., Müller, M., Gehring, W., and Wuthrich, K. (1991) *J. Mol. Biol.* **217,** 531–540
27. Cornilescu, G., Delaglio, F., and Bax, A. (1999) *J. Biomol. NMR* **13,** 289–302
28. Güntert, P., Mumenthaler, C., and Wüthrich, K. (1997) *J. Mol. Biol.* **273,** 283–298
29. Cornell, W. D., Cieplak, P., Bayly, C. I., Gould, I. R., Merz, K. M., Ferguson, D. M., Spellmeyer, D. C., Fox, T., Caldwell, J. W., and Kollman, P. A. (1995) *J. Am. Chem. Soc.* **117,** 5179–5197
30. Qi, Y., and Grishin, N. V. (2005) *Proteins* **58,** 376–388
31. Kline, A. D., Braun, W., and Wuthrich, K. (1988) *J. Mol. Biol.* **204,** 675–724
32. Ferguson, A. D., Labunskyy, V. M., Fomenko, D. E., Arac, D., Chelliah, Y., Amezcua, C. A., Rizo, J., Gladyshev, V. N., and Deisenhofer, J. (2006) *J. Biol. Chem.* **281,** 3536–3543
33. Pellecchia, M., Sem, D. S., and Wüthrich, K. (2002) *Nat. Rev. Drug Discov.* **1,** 211–219
34. Homans, S. W. (2004) *Angew. Chem. Int. Ed. Engl.* **43,** 290–300
35. Koradi, R., Billeter, M., and Wüthrich, K. (1996) *J. Mol. Graphics* **14,** 51–55
36. DeLano, W. L. (2002) *The PyMOL User's Manual*, DeLano Scientific, San Carlos, CA

Solution Structure of Selenoprotein W and NMR Analysis of Its Interaction with 14-3-3 Proteins

Finn L. Aachmann, Dmitri E. Fomenko, Alice Soragni, Vadim N. Gladyshev and Alexander Dikiy

J. Biol. Chem. 2007, 282:37036-37044.
doi: 10.1074/jbc.M705410200 originally published online October 10, 2007

Supplementary Figure 1.

2D ^{15}N HSQC spectra of reduced SelW in the presence of BSA (molar ratio 1:1.1).